ON THE RELATION OF ABOVE-THE-LOOP AND FOOTPOINT HARD X-RAY SOURCES IN SOLAR FLARES

S. Ishikawa[1,2,3], Säm Krucker[1,4], T. Takahashi[2,3], and R. P. Lin[1,5,6]

[1] Space Science Laboratory, University of California, Berkeley, CA 94720, USA; ishikawa@ssl.berkeley.edu
[2] Institute of Space and Astronautical Science, Japan Aerospace Exploration Agency, Sagamihara, Kanagawa 252-5210, Japan
[3] Graduate School of Science, University of Tokyo, Bunkyo, Tokyo 113-0033, Japan
[4] Institute of 4D Technologies, School of Engineering, University of Applied Sciences Northwestern Switzerland, 5210 Windisch, Switzerland
[5] Department of Physics, University of California, Berkeley, CA 94720-7300, USA
[6] School of Space Research, Kyung Hee University, Yongin, Gyeonggi 446-701, Republic of Korea

ABSTRACT

We report on the most prominent example of an above-the-loop hard X-ray source in the extensive solar flare database of *RHESSI*. The limb flare of 2003 October 22 around 20 UT resembles the famous Masuda flare, except that only one of the footpoint sources is visible with the other one occulted. However, even for this very prominent event, the above-the-loop source is only visible during one of the four hard X-ray peaks, highlighting the rare occurrence of above-the-loop sources that are equally bright as footpoint sources. The relative timing between the above-the-loop and footpoint sources shows that the coronal source peaks about 10 s before the footpoint source and decays during the time the footpoint source is most prominent. Furthermore, the derived number of non-thermal electrons within the above-the-loop source is large enough to provide the needed number of precipitating electrons to account for the footpoint emission over the duration of the hard X-ray peak. Hence, these observations support the simple scenario where bulk energization is accelerating all electrons within the above-the-loop source and precipitating electrons are emptying out of the above-the-loop source to produce the footpoint emissions.

Key words: Sun: flares – Sun: particle emission – Sun: X-rays, gamma rays

*Online-only material:* color figures

1. INTRODUCTION

The release of magnetic energy during solar flares is observed to be impulsive and a large fraction of the released energy goes into particle acceleration. Hard X-ray observations provide the most direct diagnostics of electron acceleration processes in solar flares. Hard X-ray emissions are most intense from the footpoints of flare loops where electrons accelerated in the corona precipitate into the much denser chromosphere-producing non-thermal bremsstrahlung emissions (see the review by Benz 2008). Hard X-ray bremsstrahlung emissions from the corona are generally much fainter, but are almost always present as well (review by Krucker et al. 2008). The most frequently cited observations of coronal hard X-ray sources are from the so-called Masuda flare (Masuda et al. 1994, 1995, 2000; Alexander & Metcalf 1997; Tomczak 2001; Petrosian et al. 2002). For this rare event, a hard X-ray source is seen above the thermal flare loop, suggesting that the energy release happens above the flare loops. High cadence studies of hard X-ray time profiles taken at different energies reveal that the observed time-of-flight delays are consistent with a coronal acceleration site located above the thermal flare loops (Aschwanden et al. 1996). Krucker et al. (2010) showed that the above-the-loop source itself is the location of particle acceleration, where all electrons are accelerated in a bulk-energization process resulting in a power-law electron population with an average energy of the order of 30 keV. However, above-the-loop hard X-ray sources are only rarely observed. This might be partially due to the limited dynamic range of present-day telescopes, but different acceleration scenarios might be present in other events. Different ideas that have been recently discussed are energy transport from the corona to the chromosphere by Alfvén waves resulting in particle acceleration in the footpoints themselves (e.g., Fletcher & Hudson 2008) and re-acceleration in footpoints (e.g., Brown et al. 2009; Turkmani & Brown 2010).

In this paper, we present the event from the *RHESSI* (Lin et al. 2002) database with the current best resemblance of the Masuda flare geometry. The good counting statistics of this event together with the imaging spectroscopy capability of *RHESSI* provide a unique opportunity for detailed spectral and temporal study of the relationship between above-the-loop and footpoint sources.

2. OBSERVATIONS

The *GOES* M9.9 flare from 2003 October 22 around 20 UT (SOL2003-10-22T20:07) that is discussed in this paper occurred in the same NOAA Active Region (AR) 10486 as the famous event of 2003 October 28 (e.g., Woods et al. 2004; Grechnev et al. 2005; Emslie et al. 2005; Hurford et al. 2006; Kiener et al. 2006; Trottet et al. 2008), one of the most energetic flares ever detected. On 2003 October 22, AR 10486 was just appearing on the eastern limb. *RHESSI* missed the onset of the flare due to spacecraft night, but showed three main hard X-ray peaks during the impulsive phase with a fourth peak occurring about 10 minutes later just after the soft X-ray peak time (Figure 1). When *RHESSI* came out of night, the count rate was already high enough so that attenuators were inserted in front of the detectors to avoid spectral distortions due to pulse pileup (Smith et al. 2002). However, it took about 40 s until both attenuators were in place. Hence, observations before 19:56:15 UT are strongly affected by pileup (46% of the counts above 30 keV
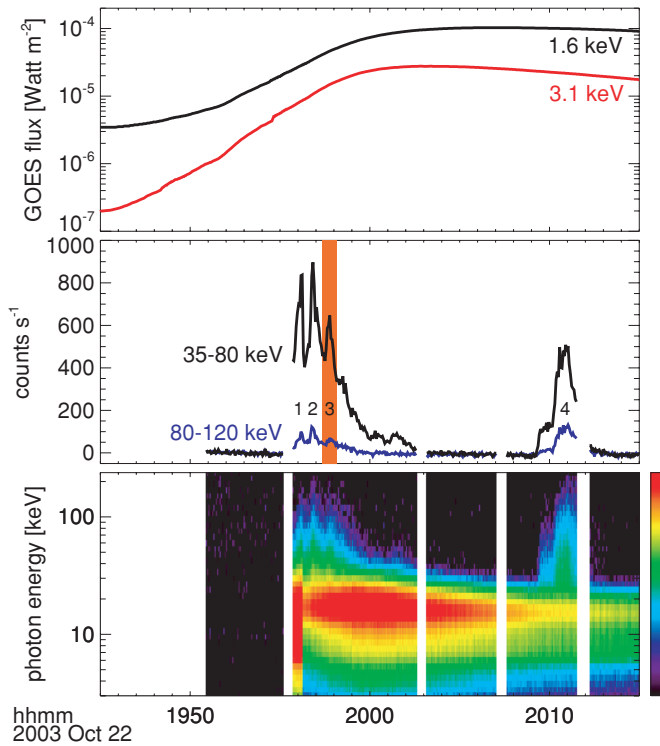
Figure 1. Time evolution of the *GOES* M9.9 class flare on 2003 October 22. From top to bottom, the time profiles of the *GOES* soft X-ray flux, the *RHESSI* hard X-ray flux in the non-thermal range, and the *RHESSI* spectrogram plot are shown. *RHESSI* missed the onset of the event and only started observing the Sun after 19:55 UT. The four hard X-ray peaks are labeled with numbers. The orange bar marks the time of the image shown in Figure 2.

(A color version of this figure is available in the online journal.)

are due to pileup). In this paper, we mainly discuss imaging and spectroscopy results of the third peak which shows an intense

above-the-loop source, and mention the imaging results of the other peaks for context (Section 2.2).

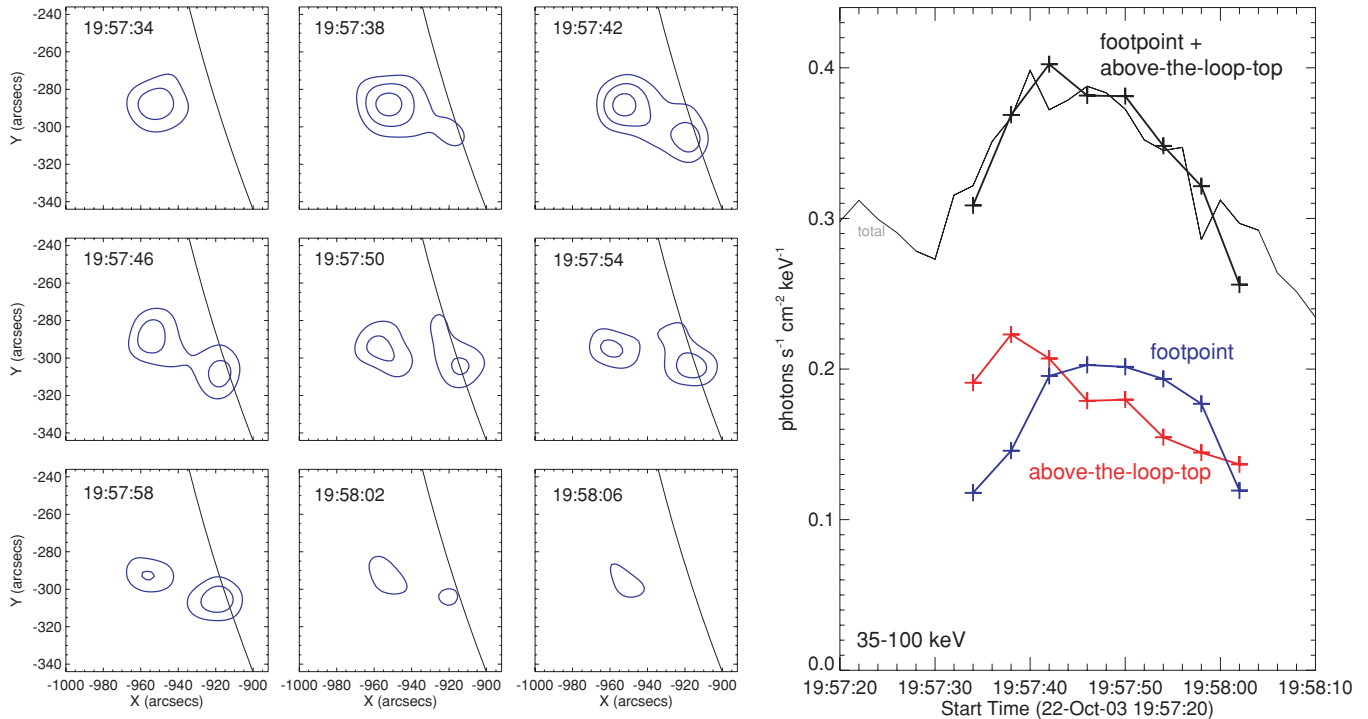### 2.1. The Above-the-loop Source Seen during Peak 3

Imaging during peak 3 reveals chromospheric footpoint emissions from a single source strongly suggesting that part of the hard X-ray emissions are occulted by the solar disk (Figure 2, left). Compared with the thermal flare loop, the observed footpoint source originates from the southern flare ribbon, with emissions from the northern ribbon occulted. Since the radius of the Sun for the extreme-ultraviolet (EUV) observations is larger than for the hard X-ray observations, the EUV images from the Extreme-Ultraviolet Imaging Telescope (EIT; Delaboudinière et al. 1995) do not show the flare ribbons at all (Figure 2, left). We considered the possibility that the observed single hard X-ray footpoint itself might be partially disk-occulted, similar to what is suspected for the Masuda flare (Wang et al. 1995). Since the thick-target beam model predicts that higher energy emissions from the footpoints originate from lower in the chromosphere (e.g., Kontar et al. 2008; Saint-Hilaire et al. 2010), partially occulted footpoints are expected to show an energy cutoff in the spectrum above which emission is occulted. However, such a behavior is not observed (see the spectrum in Figure 2, right), suggesting that the footpoint is not occulted. We therefore conclude that the single hard X-ray footpoint source that is imaged by *RHESSI* occurs at the limb, but that it is likely fully visible.

Additional to the footpoint source, an almost equally bright coronal source located about 6 Mm above the thermal flare loop is seen above 40 keV (see Figure 2, left). This event therefore strongly resembles the geometry of the Masuda flare, except that only one footpoint is seen with the other one occulted. Using the contour at half-maximum of the above-the-loop source, we find that the above-the-loop source is extended and elongated with a width of about 6 Mm and a length of 11 Mm (for details of source
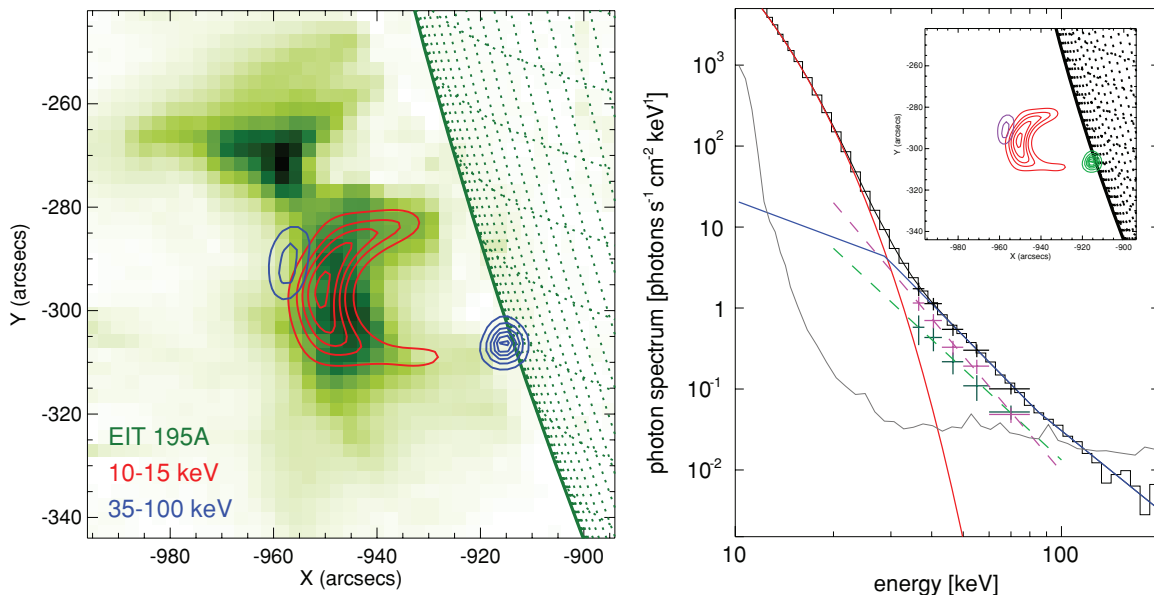
Figure 2. Left: imaging during peak 3 (19:57:30–19:58:02 UT): the *RHESSI* contours at 9–15 keV (red, thermal emission) and 35–100 keV (blue, non-thermal, PIXON image at 7″ FWHM resolution) are shown on an EIT image taken at 20:00:10 UT. Contour levels are 20%, 35%, 50%, 65%, 80%, and 95%. We note here that the observed EUV and hard X-ray emissions seen in this event strongly resemble the emissions from the partially disk-occulted event discussed in Krucker et al. (2010). Right: spectroscopy during peak 3: the spatially integrated spectrum is shown as a histogram with a thermal fit (red, $T = 33$ MK, EM $= 4.0 \times 10^{48}$ cm^{-3}) and a broken power-law fit (blue, $\gamma = 1.5, 4.1, 3.3$, break energy $= 29, 85$ keV). The thin gray curve is the background. Imaging spectroscopy results are shown in dark green for the footpoint ($\gamma_f = 3.7 \pm 0.5$) and in magenta for the above-the-loop source ($\gamma_c = 4.8 \pm 0.4$).

(A color version of this figure is available in the online journal.)

Figure 3. Relative time evolution of the above-the-loop and footpoint source during peak 3. Left: CLEANed images taken every 4 s in the energy range of 35–100 keV at low spatial resolution (17″ FWHM; subcollimators 4 and up are used with natural weighting, see Hurford et al. 2002 for details) are shown. The low spatial resolution is used to increase image quality, but to make it still possible to cleanly separate the above-the-loop and footpoint sources. The values of the contour levels are the same for all images and correspond to 50%, 70%, and 90% of the intensity of the image taken at peak time (19:57:42 UT). Right: time evolution of the footpoint (blue) and above-the-loop (red) source for peak 3 derived from 35–100 keV images. The gray curve gives the total time profile for reference.

(A color version of this figure is available in the online journal.)

size determination with *RHESSI* we refer to Dennis & Pernak 2009). Assuming a depth equal to the width, the volume of the coronal source becomes $\sim 4.0 \times 10^{26}$ cm^3. This is about a factor of four larger than the above-the-loop source in the Masuda flare and about half the size of a different above-the-loop source discussed by Krucker et al. (2010, SOL2007-12-31T00:37). *RHESSI* imaging spectroscopy (e.g., Krucker & Lin 2002; Battaglia & Benz 2006; Saint-Hilaire et al. 2008) reveals a flatter (harder) spectrum for the footpoint ($\gamma_f \sim 3.7 \pm 0.5$) than for the coronal source ($\gamma_c \sim 4.8 \pm 0.4$), similar to what is reported for the Masuda flare, if compared in the same energy range (Masuda et al. 2000). Although the uncertainty is rather large, the difference in spectral indices $\Delta\gamma = \gamma_c - \gamma_f = 1.1 \pm 0.6$ is marginally consistent with thick target emission from footpoints and thin target emission from a single electron population.

The relative time evolution of the coronal and footpoint sources is derived by making CLEANed images in the energy range of 35–100 keV (Figure 3). Despite the rather low counting statistics, the large spatial separation between the two sources of about 25 Mm makes it relatively easy to get individual flux measurements. The coronal source is found to peak earlier by about 10 s (see Figure 3, right) and decays during the time the footpoint source is visible. After 19:58:04 UT, the limited counting statistics do not allow us to accurately image both sources. The image quality available for the Masuda flare makes a detailed temporal comparison difficult. Nevertheless, the time profile shown in the original publication (Figure 2 in Masuda et al. 1994) reveals that the coronal source peaks one time bin (12 s) earlier than the footpoints. The analysis presented by Alexander & Metcalf (1997) using the PIXON algorithm for imaging does not provide high time resolution profiles, but shows that the footpoint sources are still bright while the

above-the-loop source is already decaying, similar to what is seen here. Therefore, the time evolution of the Masuda flare could be the same as for the event reported in this paper.

2.2. Earlier and Later Hard X-Ray Peaks

The first hard X-ray peak is difficult to analyze because of the large number of pulse pileup counts. For the other peaks, the above-the-loop source is not visible. Furthermore, the footpoint emission seen during peak 2 is 65″ to the north of the footpoint seen in peak 3. Hence, a different loop system seems to be flaring during peak 2, for which the southern flare ribbon is occulted. The EUV emission to the north of the main flare loop around $[-960″/-270″]$ might be related to this earlier flaring loop system. The fourth peak shows a compact footpoint from the same location as seen during peak 3, however, there is no above-the-loop source detected. The non-detection indicates that an above-the-loop source in peak 4 is at least 10 times fainter than the footpoints. This shows that above-the-loop sources are rarely observed, at least with present-day hard X-ray instruments. Even for events with a clear detection, the above-the-loop sources can be absent during other time periods despite the occurrence of bright hard X-ray footpoints. Hard X-ray focusing optics that is currently developed for solar observations (Krucker et al. 2009) will provide high enough sensitivity and dynamic range to regularly observe above-the-loop sources, if present.

3. DISCUSSION

In the following, we investigate if escaping electrons from the above-the-loop source could produce the footpoint emissions at

least for peak 3. We first estimate the number of non-thermal electrons in the above-the-loop source, and then compare it to the needed rate of precipitating electrons to produce the hard X-ray footpoint emission.

To get the number of electrons in the above-the-loop source, we adopt the interpretation from Krucker et al. (2010) that above-the-loop sources are produced by a bulk energization of all electrons to non-thermal energies. If all electrons are accelerated, the density of non-thermal electrons in the coronal source, n_c, is equal to the ambient proton density, and the instantaneous number of hard X-ray producing electrons, N_c (e.g., Lin 1974, Equation (2.4)), can be derived from the hard X-ray observations alone without the need of an independent measurement of the ambient density (see Krucker et al. 2010 for details): $N_c = 6.7 \times 10^{35}[E_0/30\,\mathrm{keV}]^{-\gamma_c/2+0.75}$ electrons above the low-energy cutoff energy E_0. We use $E_0 = 30\,\mathrm{keV}$ given by the spectral fit (Figure 2). Since this is an upper limit for E_0, the derived values here should be considered as lower limits. Using the derived volume of the above-the-loop source from above, $V \sim 4.0 \times 10^{26}\,\mathrm{cm}^3$, the density of non-thermal electrons above E_0 becomes $n_c = 1.7 \times 10^{9}[E_0/30\,\mathrm{keV}]^{-\gamma_c/2+0.75}\,\mathrm{cm}^{-3}$ with a total energy content of $E_c = 4.6 \times 10^{28}[E_0/30\,\mathrm{keV}]^{-\gamma_c+1.75}$ erg.

Using the standard thick-target approximation (e.g., Brown 1971) and the spectral fit to the footpoint emission (Figure 2, right), the energy-loss rate of energetic electrons precipitating into the chromosphere becomes $\epsilon_f = 1.8 \times 10^{27}[E_0/30\,\mathrm{keV}]^{-\gamma_f+1}$ erg s^{-1} provided by $\mathcal{N}_f = 2.7 \times 10^{34}[E_0/30\,\mathrm{keV}]^{-\gamma_f}$ electrons per second above E_0.

It is now straightforward to calculate how long the coronal source would last if it had to provide the electrons precipitating into the footpoint: $\tau \equiv N_c/\mathcal{N}_f \sim 24[E_0/30\,\mathrm{keV}]^{-\gamma_f+\gamma_c/2+0.75}$ s (we note here that, contrarily to N_c and N_f, τ does not heavily depend on E_0). Since only one footpoint is seen with the second footpoint occulted, τ is expected to be smaller than what is given above. Since equally bright footpoints are most commonly observed (e.g., Saint-Hilaire et al. 2008), we adopt a factor of two, giving τ of the order of 12 s. Hence, the derived timescale is of the same order as the observed e-folding time of the coronal source of $\sim$20 s (Figure 1, right). Together with the time evolution, this indicates that the simple model whereby the above-the-loop provides the electrons seen in the footpoint sources could work.

Since the observed spectral difference $\Delta\gamma = \gamma_c - \gamma_f = 1.1 \pm 0.6$ is within the uncertainties of the expected difference between the thin- and thick-target models, the spectral distribution of the electrons in the above-the-loop and in the footpoints could be the same if the escape is assumed to be energy-independent. However, the large uncertainty in $\Delta\gamma$ does not provide strong constraints on the energy dependence of the escape probability. Furthermore, transport effects can influence the spectral shape as well (e.g., Battaglia & Benz 2007, 2008; Zharkova et al. 2010). Statistics are not good enough to find significant spectral changes in time.

A further simple test of this model is to estimate the hard X-ray emission that is produced by the precipitating electrons between the above-the-loop and the footpoint sources. To derive the emission from the leg of the flare loop, we assume the same ambient density in the above-the-loop source as in the legs of the loop and an energy-independent escape. The ratio of the hard X-ray emission produced in the above-the-loop source to the emission in the legs of the flare loop is then proportional to the ratio of time electrons stay in the above-the-loop source, Δt_c, and the electron transit time from the corona to the footpoint,

Δt_f. From the observations we get an average Δt_c of the order of 10 s (half the total duration of peak 3). The transit time of electrons with an energy of 30 keV (loop length is about 25 Mm) is $\sim$0.2 s times a factor larger than one for the pitch angle dependence. Since $\Delta t_c \gg \Delta t_f$, the emission from the legs of the loop is expected to be much fainter than the emission of the above-the-loop source. Even for a very large pitch angle and additionally including magnetic mirroring to enlarge the transit time, the limited dynamic range of the *RHESSI* observations (of five for complex images such as expected here) is likely not able to detect hard X-ray emission from the leg of the loop.

4. SUMMARY

Good examples of above-the-loop sources similar to the Masuda flare are rare even in the extensive *RHESSI* database (e.g., Krucker & Lin 2008). Nevertheless, *RHESSI* observations clearly confirm the existence of this type of source (e.g., Sui et al. 2004; Krucker et al. 2010; Petrosian & Chen 2010). In this paper, we report on the currently best example of a *RHESSI* flare that resembles the Masuda flare geometry. *RHESSI*'s imaging spectroscopy capability allows us to study the timing and energetics of the above-the-loop source relative to the footpoints with much better accuracy than before. In particular, we report for the first time a detailed temporal and spectral comparison between the above-the-loop and footpoint sources.

The above-the-loop source is observed to peak about 10 s earlier than the footpoint sources and decays afterwards while the footpoint source stays bright. This suggests that the above-the-loop source provides the precipitating electrons that feed the footpoint source. To make a more quantitative comparison we estimate the number of non-thermal electrons in the above-the-loop source and compare this to the needed precipitation rate of non-thermal electrons to produce the hard X-ray emission in footpoint source. The largest uncertainty in this derivation is introduced by the unknown fraction of occulted hard X-ray footpoint emission. However, assuming that half the emission is occulted, the timescale to empty out the above-the-loop source is of the same order of magnitude as the duration of the footpoint emission. Hence, there are enough electrons within the above-the-loop source to account for the footpoint emission. We therefore put forward the following scenario: magnetic energy release within the above-the-loop source produces a bulk energization and accelerates all electrons to energies of tens of keV, and electrons escaping the above-the-loop source then produce the footpoint emission. Both the acceleration and the escape mechanism are currently not understood. The interplay between acceleration efficiency and escape probability are important parameters for the creation of an above-the-loop source. If the escape probability is large compared to the acceleration efficiency, a bulk energization does not happen as accelerated electrons precipitate too quickly. Hence, the rare cases where we observe intense above-the-loop sources could be events where the escape probability is low (e.g., trapping of accelerated electrons within the acceleration region is efficient) compared to the acceleration efficiency.

REFERENCES

Alexander, D., & Metcalf, T. R. 1997, ApJ, 489, 442
Aschwanden, M. J., Hudson, H., Kosugi, T., & Schwartz, R. A. 1996, ApJ, 464, 985
Battaglia, M., & Benz, A. O. 2006, A&A, 456, 751
Battaglia, M., & Benz, A. O. 2007, A&A, 466, 713
Battaglia, M., & Benz, A. O. 2008, A&A, 487, 337
Benz, A. O. 2008, Living Rev. Sol. Phys., 5, 1
Brown, J. C. 1971, Sol. Phys., 18, 489
Brown, J. C., Turkmani, R., Kontar, E. P., MacKinnon, A. L., & Vlahos, L. 2009, A&A, 508, 993
Delaboudinière, J.-P., et al. 1995, Sol. Phys., 162, 291
Dennis, B. R., & Pernak, R. L. 2009, ApJ, 698, 2131
Emslie, A. G., Dennis, B. R., Holman, G. D., & Hudson, H. S. 2005, J. Geophys. Res., 110, 11103
Fletcher, L., & Hudson, H. S. 2008, ApJ, 675, 1645
Grechnev, V. V., et al. 2005, J. Geophys. Res.: Space Phys., 110, 9
Hurford, G. J., Krucker, S., Lin, R. P., Schwartz, R. A., Share, G. H., & Smith, D. M. 2006, ApJ, 644, L93
Hurford, G. J., et al. 2002, Sol. Phys., 210, 61
Kiener, J., Gros, M., Tatischeff, V., & Weidenspointner, G. 2006, A&A, 445, 725
Kontar, E. P., Dickson, E., & Kašparová, J. 2008, Sol. Phys., 252, 139
Krucker, S., Hudson, H. S., Glesener, L., White, S. M., Masuda, S., Wuelser, J.-P., & Lin, R. P. 2010, ApJ, 714, 1108
Krucker, S., & Lin, R. P. 2002, Sol. Phys., 210, 229
Krucker, S., & Lin, R. P. 2008, ApJ, 673, 1181
Krucker, S., et al. 2008, A&AR, 16, 155
Krucker, S., et al. 2009, Proc. SPIE, 7437, 743705
Lin, R. P. 1974, Space Sci. Rev., 16, 189
Lin, R. P., et al. 2002, Sol. Phys., 210, 3
Masuda, S., Kosugi, T., Hara, H., Sakao, T., Shibata, K., & Tsuneta, S. 1995, PASJ, 47, 677
Masuda, S., Kosugi, T., Hara, H., Tsuneta, S., & Ogawara, Y. 1994, Nature, 371, 495
Masuda, S., Sato, J., Kosugi, T., & Sakao, T. 2000, Adv. Space Res., 26, 493
Petrosian, V., & Chen, Q. 2010, ApJ, 712, L131
Petrosian, V., Donaghy, T. Q., & McTiernan, J. M. 2002, ApJ, 569, 459
Saint-Hilaire, P., Krucker, S., & Lin, R. P. 2008, Sol. Phys., 250, 53
Saint-Hilaire, P., Krucker, S., & Lin, R. P. 2010, ApJ, 721, 1933
Smith, D. M., et al. 2002, Sol. Phys., 210, 33
Sui, L., Holman, G. D., & Dennis, B. R. 2004, ApJ, 612, 546
Tomczak, M. 2001, A&A, 366, 294
Trottet, G., Krucker, S., Lüthi, T., & Magun, A. 2008, ApJ, 678, 509
Turkmani, R., & Brown, J. 2010, arXiv:1011.0756
Wang, H., Gary, D. E., Zirin, H., Kosugi, T., Schwartz, R. A., & Linford, G. 1995, ApJ, 444, L115
Woods, T. N., et al. 2004, Geophys. Res. Lett., 31, 10802
Zharkova, V. V., Kuznetsov, A. A., & Siversky, T. V. 2010, A&A, 512, A8